npj | precision oncology

Article

Published in partnership with The Hormel Institute, University of Minnesota

https://doi.org/10.1038/s41698-024-00663-1

TKI type switching overcomes ROS1 L2086F in ROS1 fusion-positive cancers

Rajat Thawani[1,6], Matteo Repetto[2,6], Clare Keddy[3], Katelyn Nicholson[3], Kristen Jones[3], Kevin Nusser[3], Catherine Z. Beach[3], Guilherme Harada[2], Alexander Drilon[2,4] ✉ & Monika A. Davare[3,5] ✉

The grammar in this abstract is generally correct, but there's a minor issue with sentence structure in one part. Here's a slightly revised version with improved grammar and flow:
ROS1 tyrosine kinase inhibitors (TKIs) are highly effective in ROS1-positive non-small cell lung cancer, but resistance remains a challenge. We investigated the activity of various TKIs against wildtype and mutant ROS1, focusing on the emerging L2086F resistance mutation. Using Ba/F3 and NIH3T3 cell models, CRISPR/Cas9-edited isogenic wildtype and mutant patient-derived cell lines, and in vivo tumor growth studies, we compared type I TKIs (crizotinib, entrectinib, taletrectinib, lorlatinib, and repotrectinib) to type II TKIs (cabozantinib and merestinib) and the type I FLT3 inhibitor gilteritinib. The ROS1 L2086F mutant kinase showed resistance to type I TKIs, while type II TKIs retained activity. Gilteritinib inhibited both wildtype and L2086F mutant ROS1 but was ineffective against the G2032R mutation. Structural analyses revealed distinct binding poses for cabozantinib and gilteritinib, explaining their efficacy against L2086F. Clinical cases demonstrated cabozantinib's effectiveness in patients with TKI-resistant, ROS1 L2086F mutant NSCLCs. This study provides the first comprehensive report of ROS1 L2086F in the context of later-generation TKIs, including macrocyclic inhibitors. While cabozantinib effectively inhibits ROS1 L2086F, its multi-kinase inhibitor nature highlights the need for more selective and better-tolerated TKIs to overcome kinase-intrinsic resistance. Gilteritinib may offer an alternative for targeting ROS1 L2086F with distinct off-target toxicities, but further studies are required to fully evaluate its potential in this setting.

Chromosomal rearrangements involving the protooncogene and receptor tyrosine kinase (RTK) *ROS1* generate catalytically active ROS1 fusion oncoproteins[1]. Patients with *ROS1* fusion-containing cancers display exquisite and durable sensitivity to small molecule ROS1 tyrosine kinase inhibitors (TKIs).

TKIs are broadly classified based on their preferred binding mode within the kinase domain. Kinase domains have evolved to adopt a common two-lobe fold (N- and C-l) connected by a hinge. ATP binds within a pocket created between the N- and C-lobes and the conformation of the activation loop (A-loop), which is marked by a conserved Asp-Phe-Gly ("DFG") motif at its start. In the active conformation, the DFG motif orients towards the ATP-binding site, whereas in the inactive conformation, the DFG motif is flipped to create a catalytically incompetent state unfavorable for ATP binding. Notably, in the DFG-out kinase conformation, a new allosteric binding pocket adjacent to the ATP binding pocket, is observed. Generally, TKI that occupy the ATP binding pocket are classified as type I or ATP-competitive inhibitors. Among ROS1 TKI, crizotinib, taletrectinib, lorlatinib, repotrectinib and NVL-520 are ATP-competitive type I inhibitors. We previously showed that entrectinib exhibits varying degrees of resistance to ROS1 kinase domain mutations associated with both type I TKI resistance (e.g., ROS1 G2032R) and type II TKI resistance (e.g., ROS1 F2004C), thus suggesting that entrectinib is potentially a type I/II inhibitor with dual binding mode potential[2]. We previously established that the multi-kinase inhibitor, cabozantinib, operates as a type II ROS1 TKI and is liable to resistance with ROS1 D2113N/G, F2004C, and F2075C kinase domain mutations[3]. These resistance mutations have not been observed with type I

[1]Section of Hematology/Oncology, Department of Medicine, University of Chicago, Chicago, IL, 60637, USA. [2]Thoracic Oncology Service, Division of Solid Tumor Oncology, Department of Medicine, Memorial Sloan Kettering Cancer Center, Weill Cornell Medical College, New York, NY, 10065, USA. [3]Department of Pediatrics, Oregon Health & Science University, Portland, OR, 97239, USA. [4]Weill Cornell Medical College, New York, NY, USA. [5]Knight Cancer Institute, Oregon Health & Science University, Portland, OR, 97239, USA. [6]These authors contributed equally: Rajat Thawani, Matteo Repetto. ✉e-mail: drilona@mskcc.org; davarem@ohsu.edu

inhibitors, supporting the unique binding pocket requirements for the inhibitors.

In TKI-naïve ROS1 fusion-containing NSCLCs, the three approved ROS1 TKIs (crizotinib, entrectinib, and repotrectinib) achieve high response rates (70-80%) and prolonged progression-free survival (PFS)[4–6]. Next-generation TKIs such as repotrectinib[7], taletrectinib[8–10], and NVL-520[11] were designed to target solvent front resistance arising from the recurrent crizotinib and entrectinib-resistant ROS1 G2032R mutation, with clinical responses to these to these second-line agents now reported in patients with ROS1 G2032R. Furthermore, repotrectinib is now a first line TKI option, achieving a longer median PFS in this setting compared to crizotinib or entrectinib (~36 months vs ~16 months for both drugs).

The acquired resistance landscape is likely to adapt to the increasing use of next-generation TKIs. Kinase-intrinsic resistance is typically mediated by the acquisition of *ROS1* mutations with steric, functional, or conformational consequences. We previously reported data from a cohort of patients with *ROS1*-rearranged NSCLC treated with crizotinib and lorlatinib, a National Cancer Center Network Guidelines listed but unapproved ROS1 TKI[12]. The ROS1 G2032R solvent front mutation was most commonly observed. Next-generation TKIs with anti-ROS1 G2032R activity remain type I inhibitors, interacting with the ATP binding site within the kinase's active pocket like older drugs. As such, resistance mechanisms that broadly affect type I inhibitors may become more clinically relevant.

We and others observed the emergence of on-target resistance due to ROS1 L2086F in *ROS1* fusion-containing cancers treated with both earlier-generation (crizotinib, entrectinib and lorlatinib[12]) and next-generation (taletrectinib) ROS1 TKIs[2,12,13]. Lin et al. reported ROS1 L2086F mutations emerging either alone or as complex mutations in ~10% of crizotinib- and/or lorlatinib-resistant patients[12]. However, with next-generation ROS1 TKIs such as repotrectinib, taletrectinib and NVL-520 that mitigate the recurrent ROS1 G2032R resistance, the prevalence of L2086F is likely to increase[14,15].

Amino acid L2086 corresponds to the catalytic spine 6 (CS6) residue of ROS1[16]. This residue is functionally conserved across tyrosine kinases and forms a crucial part of the ATP-binding pocket floor. It plays a key role in forming hydrophobic interactions with the adenine base of ATP. ROS1 L2086F is a CS6 mutation. This mutation appears to disrupt type I TKI binding of clinically approved type I ROS1 TKIs. Interestingly, it shares many similarities with its paralog, the ALK CS6 mutation L1256F[17]. As a result, ROS1 L2086F may become a prevalent kinase-intrinsic resistance liability, potentially replacing the well-known ROS1 G2032R resistance mutation. Given this potential impact, we aimed to characterize ROS1 L2086F and describe therapeutic strategies for managing this mutation

Results

Assessing the activity of ROS1 Inhibitors with distinct binding modes in TKI-resistant ROS1 mutants

Using dose-response cell viability assays in Ba/F3 CD74-ROS1 wild-type and ROS1 F2004C, L2026M, G2032R and L2086F kinase domain mutant cell lines, we determined the cell-based 50% inhibitory concentration (IC_{50}) for type I TKI (crizotinib, entrectinib, taletrectinib, lorlatinib, and repotrectinib), and type II TKI (cabozantinib, merestinib), and the type I FLT3 inhibitor, gilteritinib that was recently shown to have activity in ALK fusion driven cancer models[18] (Fig. 1a, Supplementary Fig. 1). As anticipated, older ROS1 inhibitors exhibited loss of potency in cells with the ROS1 G2032R mutation, while next-generation TKIs, taletrectinib and repotrectinib maintained activity. The cell-based IC_{50} for CD74-ROS1 ROS1 L2086F was 50-500-fold higher compared to CD74-ROS1 ROS1 wildtype kinase. Thus, ROS1 L2086F unequivocally represents a resistance liability for all established type I ROS1 TKIs. ROS1 L2086F exhibits modest hypersensitivity to cabozantinib, merestinib, and gilteritinib, with these inhibitors demonstrating a lower IC_{50} for ROS1 L2086F than for ROS1 wildtype cells. Despite inhibition of L2086F, gilteritinib is resistant to ROS1 G2032R, similar to other type I TKIs. This finding confirms that akin to its binding to FLT3, gilteritinib likely favors a type I binding mode for DFG-in ROS1. Furthermore, consistent with our previous observations[3] showing that the F2004C mutation confers resistance to type II TKIs like cabozantinib and foretinib, we now confirm that in addition to cabozantinib and foretinib, the type II TKI merestinib is also resistant to ROS1 F2004C. A network diagram summarizing the kinase-intrinsic resistance liabilities for all tested TKIs, based on dose-response cell viability assay data, is presented in Fig. 1b.

Immunoblotting was used to explore the on-target activity of cabozantinib and gilteritinib as these drugs demonstrated robust cell-based growth inhibition of cells harboring ROS1 L2086F (Fig. 1c). In both Ba/F3 CD74-ROS1 wildtype and L2086F mutant cells, both inhibitors effectively reduced ROS1 autophosphorylation, aligning with their potency observed in Ba/F3 cell viability assays. Cabozantinib reduced autophosphorylation in ROS1 G2032R, whilst gilteritinib was not effective in this mutant, also consistent with cell viability data.

Sequential treatment with kinase inhibitors risks the emergence of compound mutations, as has been observed initially in the case of imatinib-treated BCR-ABL positive chronic myeloid leukemia, and in EGFR- or ALK-driven lung cancer[19–21]. With advancing next-generation second- and third-line therapeutics for ROS1, complex or compound mutations may arise in this context. To explore inhibitor sensitivity of compound mutations in ROS1, we engineered two mutant CD74-ROS1 kinases where the two mutations are within the same protein molecule: F2004C + L2086F and G2032R + L2086F. Dose response cell viability analysis indicated that type-specific resistance mutations (F2004C is resistant to cabozantinib and G2032R to gilteritinib) influenced inhibitor effectiveness alongside the L2086F mutant protein (Fig. 1d, Supplementary Fig. 2). Notably, cells harboring the F2004C + L2086F mutation maintained sensitivity solely to gilteritinib. Similarly, G2032R + L2086F cells were only responsive to cabozantinib.

To confirm the activities of cabozantinib and gilteritinib in an independent model system, we performed soft-agar colony formation assays with NIH3T3 CD74-ROS1 cell lines (WT and L2086F) comparing treatments with entrectinib. Dose dependent inhibition of WT colonies with entrectinib, cabozantinib and gilteritinib was observed (Fig. 1e). ROS1 L2086F colony formation was resistant to entrectinib but sensitive to cabozantinib and gilteritinib (Fig. 1f, Supplementary Fig. 3a, b. Similar results were observed in cell lines expressing the EZR-ROS1 fusion (Supplementary Fig. 3c–f). Further, we tested the in vivo anti-tumor efficacy of cabozantinib and gilteritinib using NIH3T3 CD74-ROS1 WT and L2086F mutant subcutaneous allograft models. Tumor bearing mice were treated with 30 mg/kg cabozantinib or gilteritinib, once daily, and compared to vehicle treatment. This dosing strategy was consistent with previous murine model studies using these agents[18,22]. Cabozantinib and gilteritinib treatments significantly inhibited the growth of both WT ROS1 and ROS1 L2086F tumors ($p < 0.05$ as indicated, Supplementary Fig. 4).

Comparative inhibitor responses in a patient-derived cell line expressing endogenous L2086F mutation

Currently, there are no patient-derived *ROS1* fusion-positive cell lines harboring the L2086F resistance mutation. CUTO-28 is a previously established TPM3–ROS1-fusion-expressing, patient-derived NSCLC cell line with sensitivity to ROS1 TKIs[23]. We used CRISPR-Cas9 genome editing coupled with homology-directed repair (HDR) to generate isogenic ROS1 WT and L2086F mutant CUTO-28 cell lines. The endogenous ROS1 L2086F mutation within TPM3-ROS1, and its expression was confirmed using Sanger sequencing of amplicons generated from gDNA and cDNA harvested from the engineered cells (Supplementary Fig. 5). We used the bulk population of edited cells for subsequent studies.

We compared the efficacy of the panel of inhibitors tested in the Ba/F3 mutant models, crizotinib, entrectinib, lorlatinib, taletrectinib repotrectinib, cabozantinib, merestinib, and gilteritinib in CUTO28 parental (with ROS1 wildtype kinase domain) and CUTO-28 L2086F mutant cells using dose-response cell viability assays (Fig. 2a, Supplemental Fig. 6a). Figure 2b depicts a 10- to 1000-fold change in the cell-based IC_{50} of crizotinib, entrectinib, lorlatinib, taletrectinib, and repotrectinib in the CUTO-28 ROS1 L2086F cells relative to CUTO-28 parental cells. Cabozantinib,

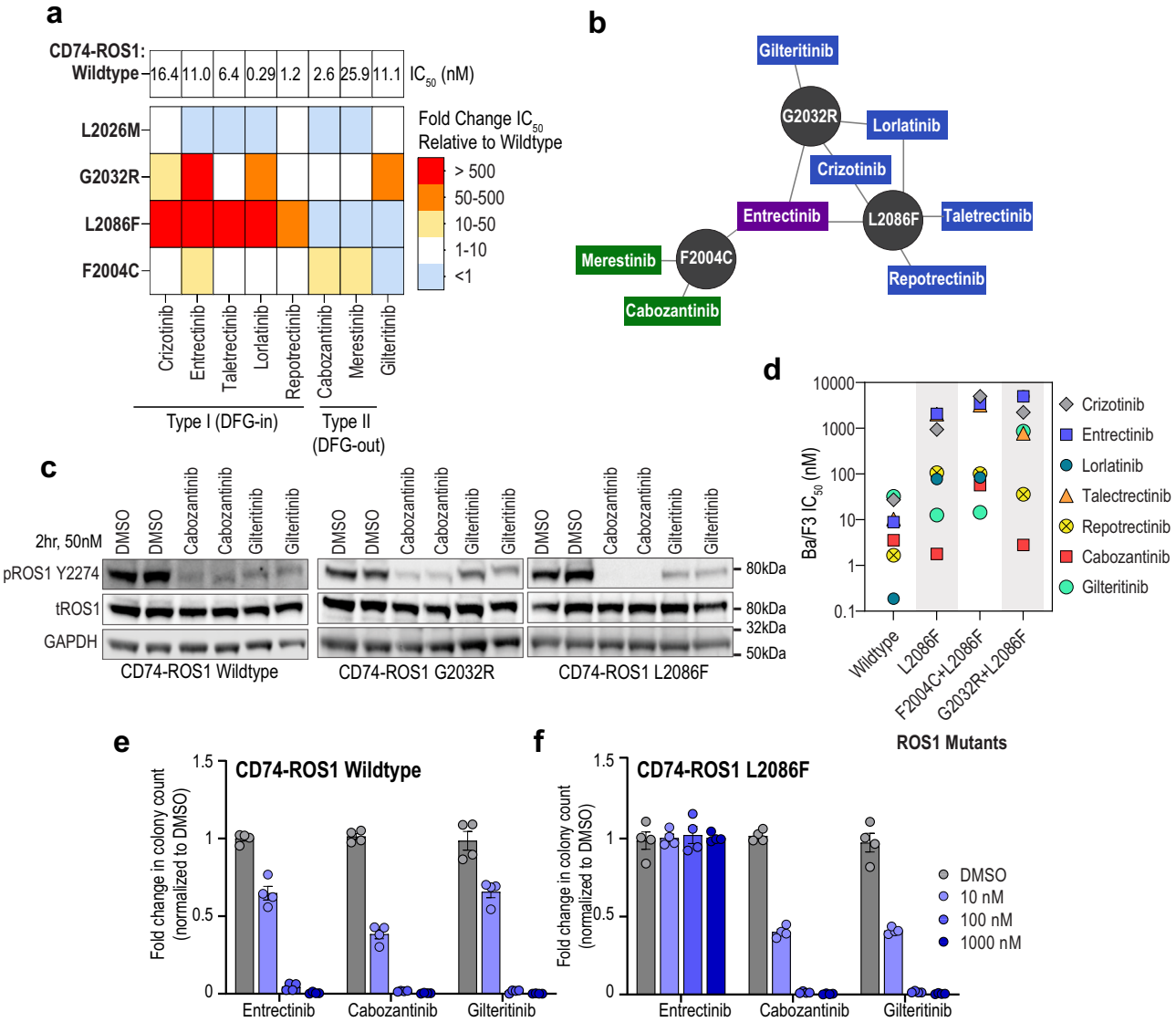

Fig. 1 | TKI activity in models of ROS1 kinase-intrinsic resistance. a Heat map of IC_{50} values shows relative potency (nM) of the indicated ROS1 inhibitors for Ba/F3 *CD74-ROS1* wildtype and mutant cell lines. IC_{50} values were calculated from three replicates from two independent experiments. **b** Network diagram summarizes tyrosine kinase inhibitor (TKI) activity against ROS1 G2032R, L2086F, and F2004C mutants, with type I inhibitors shown in blue, type II in green, and type I/II in purple. **c** Immunoblot analysis of phosphorylated and total ROS1 in cell lysates generated from Ba/F3 *CD74-ROS1* wildtype, G2032R, and L2086F cell lines treated with indicated inhibitors at 50 nM for 2 h. **d** Scatter plot of cell-based IC50 values for Ba/F3 CD74-ROS1 wildtype, L2086F, F2004C + L2086F, and G2032R + L2086F cell lines tested with crizotinib, entrectinib, lorlatinib, taletrectinib, repotrectinib, cabozantinib and gilteritinib. **e**, **f** Colony counts anchorage-independent soft agar assays using NIH3T3 *CD74-ROS1* WT (**e**) and L2086F (**f**) cell lines. Data normalized to vehicle (DMSO) treatment for indicated TKI treatment conditions. Average and standard error of means is shown in graphs ($N = 4$).

merestinib and gilteritinib retained comparable activity in the wildtype and L2086F mutant cells. CUTO-28 Control HDR (wildtype ROS1) cells remain unaffected by the mock genome editing process.

We assessed the on-target activity of cabozantinib and gilteritinib in comparison to crizotinib and lorlatinib. Initially, we used a static inhibitor dose of 100 nM for a 4-h treatment. As depicted in the immunoblots in Fig. 2c, both cabozantinib and gilteritinib treatments reduced ROS1 autophosphorylation in both the parental CUTO-28 (wildtype kinase domain) and TPM3–ROS1 L2086F cells. As previously reported, ROS1 L2086F confers resistance to crizotinib and lorlatinib. The corresponding inhibition of downstream effectors (SHP2, ERK1/2, STAT3, and S6) correlated with the extent of ROS1 auto-inhibition (Fig. 2c). Gilteritinib's modest activity at the 100 nM drug dose may reflect its inherently lower potency to inhibit ROS1 compared to cabozantinib, as evidenced by its cell-based growth inhibitor IC_{50}s of 133 for the wildtype kinase.

To compare the pharmacodynamic on-target activity and potency of cabozantinib and gilteritinib with entrectinib, we treated cells with an expanded range of inhibitor doses for 4 h, as indicated in Fig. 2d. ROS1 L2086F was inhibited by ≥90% with 25 nM cabozantinib, whereas the mutant required a 10-fold higher gilteritinib concentration of 250 nM for ≥90% inhibition. As expected, entrectinib was an ineffective inhibitor of ROS1 L2086F autophosphorylation, even at doses as high as 2500 nM.

To assess the persistence of inhibitor response, we conducted time-course studies using a 25 nM dose of entrectinib, cabozantinib, and gilteritinib on both CUTO-28 parental and CUTO-28 ROS1 L2086F cell lines (Fig. 2e). At this dose, entrectinib exhibited increasing inhibition of wildtype ROS1 fusion for up to 4 h, followed by a partial loss of inhibition after 6 h. A similar trend was observed for pERK (MAPK) (Supplementary Fig. 6b). ROS1 L2086F mutant displayed expected resistance to entrectinib

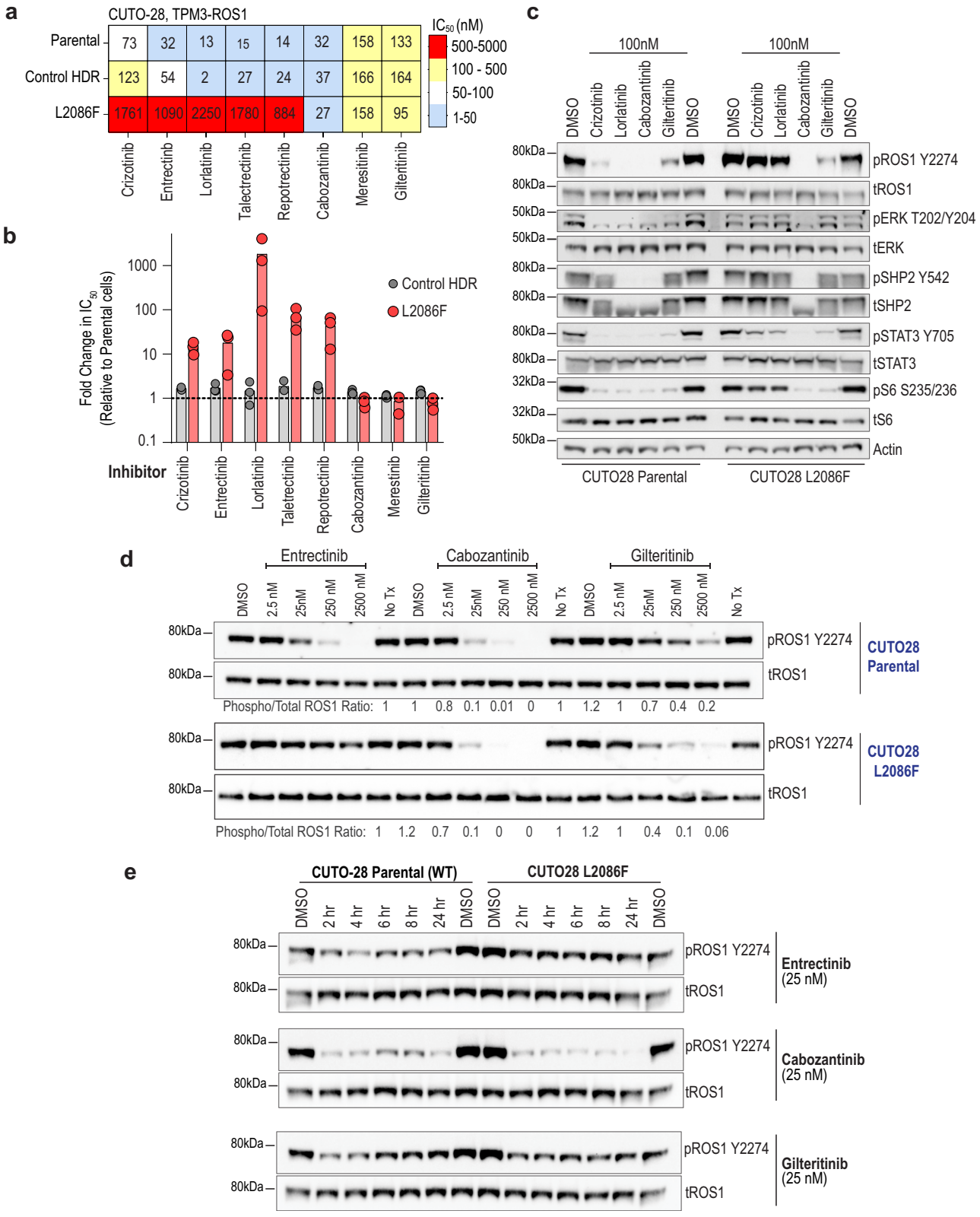

inhibition. Cabozantinib achieved maximal inhibition of wildtype cells at 4 h, with modest increase in phospho-ROS1 observed at 6 and 8 h of treatment. Interestingly, cabozantinib maintained prolonged inhibitory effects on the ROS1 L2086F mutant protein for up to 24 h of treatment. Gilteritinib activity was akin to cabozantinib, with the re-emergence of some phospho-ROS1 after 4 h of continuous treatment in wild-type cells, but not in mutant cells. Supplementary Fig. 6c, d illustrate the impact of cabozantinib and gilteritinib treatments on the activation of effector proteins (ERK1/2 and S6), respectively. These results suggest that compensatory feedback mechanisms, independent of ROS1 activity, may facilitate the reactivation of phospho-ERK1/2, but not phospho-S6, in the context of TKI treatments extending beyond 6 h.

Fig. 2 | Activity of ROS1 inhibitors in CUTO-28 patient-derived *TPM3–ROS1* fusion cell line with or without L2086F. a Heat map depicting IC_{50} data from dose response cell viability assays conducted using CUTO-28 *TPM3–ROS1* fusion parental or L2086F cell lines. Colorimetric reagent CCK-8 was added after 72-h exposure with varying concentrations of crizotinib, cabozantinib, repotrectinib, or gilteritinib. Absorbance data were normalized to vehicle-treated cells. **b** Fold change in IC_{50} of indicated inhibitors is graphed relative to the Parental Cell IC_{50}. Control HDR indicates the CUTO-28 cell line that was subjected to genome editing; however, instead of L2086F editing, the HDR template retained wildtype amino acid. **c** Immunoblot analysis of phosphorylated and total ROS1, ERK, and downstream pathways in cell lysates generated from CUTO-28 parental and TPM3-ROS1 L2086F cells treated with indicated inhibitors at 100 nM for 4 h. **d** Immunoblot analysis of phosphorylated and total ROS1 from lysates generated from CUTO-28 parental and TPM3-ROS1 L2086F cells after 4 h treatment with DMSO (Vehicle) or 2.5, 25, 250, 2500 nM concentrations of entrectinib, cabozantinib and gilteritinib, as indicated. The ratio of phosphorylated ROS1 divided by total ROS1 as determined by densitometry is presented below the blots. **e** Immunoblot analysis of phosphorylated and total ROS1 from lysates generated from CUTO-28 parental and TPM3–ROS1 L2086F cells that were treated for 2, 4, 6, 8, and 24 h with 25 nM entrectinib, cabozantinib and gilteritinib, as indicated.

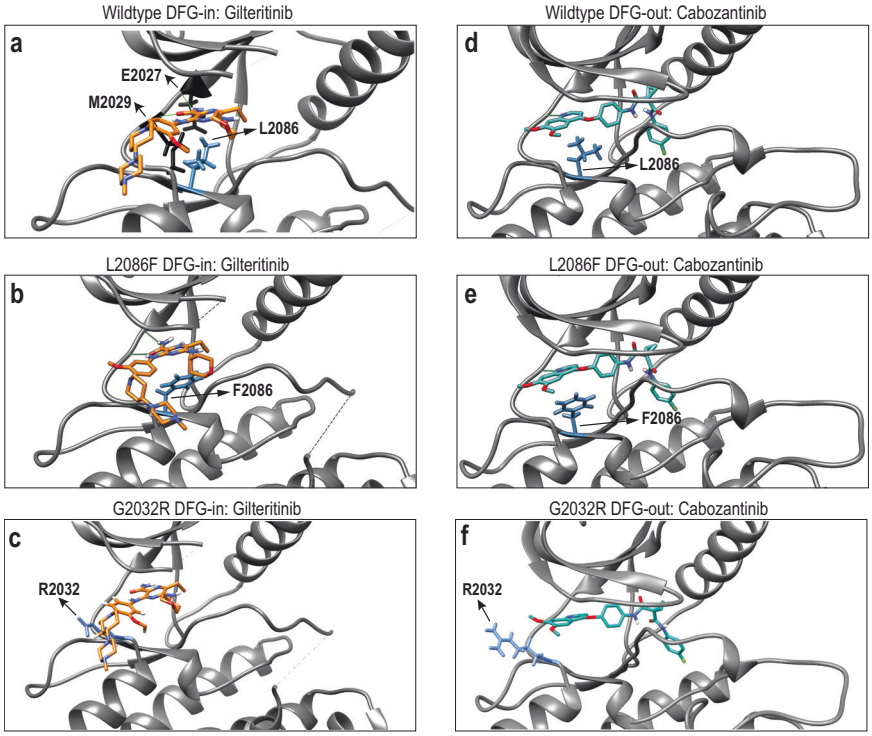

Fig. 3 | Molecular docking of gilteritinib and cabozantinib to wild-type and mutant ROS1. a Model of wild-type ROS1 kinase domain with gilteritinib in a type I conformation. L2086 is shown in blue, and gilteritinib is shown in orange. **b** Model of ROS1 L2086F kinase domain with gilteritinib bound in a type I conformation. F2086 is shown in blue, and gilteritinib is shown in orange. **c** Model of ROS1 G2032R bound to gilteritinib in the type I (DFG-in) conformation. Predicted steric clash between R2032 and gilteritinib is depicted. **d** Model of wild-type ROS1 kinase domain bound to with cabozantinib bound in the type II conformation. L2086 is shown in blue, and cabozantinib is shown in teal. **e** Model of ROS1 L2086F kinase domain bound to cabozantinib in the type II conformation. F2086 is shown in blue, and cabozantinib is shown in light teal. **f** Model of ROS1 G2032R bound to cabozantinib in the type II conformation.

Molecular docking exploration of non-type I TKI interactions with ROS1 wildtype and L2086F mutant kinases

Given the unique pharmacology of gilteritinib compared to type I and type II TKIs, we conducted molecular docking simulation studies to understand the structural basis of the activity of gilteritinib and cabozantinib in ROS1 WT and mutant kinases (Fig. 3). The studies used the previously reported crystal structure of ROS1 DFG-in kinase (PDB 3ZBF) and homology models of ROS1 DFG-out based on a reported crystal structure of DFG-out ALK (PDB 4FNY). Homology models of ROS1 G2032R and L2086F mutants were also generated.

The docking of gilteritinib on DFG-in ROS1 was successful for both WT DFG-in ROS1 (Fig. 3a) and ROS1 L2086F (Fig. 3b). The model showed that the pyrazine-2-carboxamide moiety of gilteritinib forms two hydrogen bonds with the peptide backbone of both E2027 (H1) and M2029 (H3) in the hinge region of ROS1[24]. This conformation was comparable to those observed in the reported crystal structures of gilteritinib bound to MERTK (PDB 7AB1) and to FLT3 (PDB 6JQR)[25]. This ROS1-giltertinib docked model predicted that gilteritinib occupies the adenosine-binding pocket, the ribose pocket, and the solvent-front cleft of ROS1, confirming it as a type I inhibitor, akin to its reported binding of FLT3. Consistent with cell-based experiments, the bulky R2032 residue from the G2032R solvent-front mutation disrupt optimal gilteritinib binding as it induces steric clash and blocks gilteritinib's access to the solvent-front cleft (Fig. 3c), thus making it an ineffective inhibitor for ROS1 G2032R. We subsequently evaluated the distance between the nearest aromatic system of gilteritinib and the aromatic sidechain of ROS1 L2086F. Using Pymol's ring distance measurement function, we found that the center of the pyrazinamide moiety of gilteritinib is predicted to be 4.0 Å away from the center of the F2086 residue's aromatic ring. This is within range to hypothesize a gain in π–π interaction between gilteritinib and the mutant protein[26,27] (Supplementary Fig. 7).

As we previously showed, cabozantinib docking was successful on the DFG-out conformation of wildtype ROS1 (Fig. 3d) and with the ROS1 L2086F (Fig. 3e) and G2032R (Fig. 3f) mutants. These models show that the quinoline moiety of cabozantinib forms a hydrogen bond with the H1 residue of ROS1 and extends from the adenosine binding pocket to the back-pocket of the kinase, without substantial extension into the solvent-front cleft. Evaluating the relationship between the center of the quinoline moiety of cabozantinib and the aromatic ring introduced by the L2086F showed that these aromatic systems also lie at a distance of 4.0 Å, within predictive

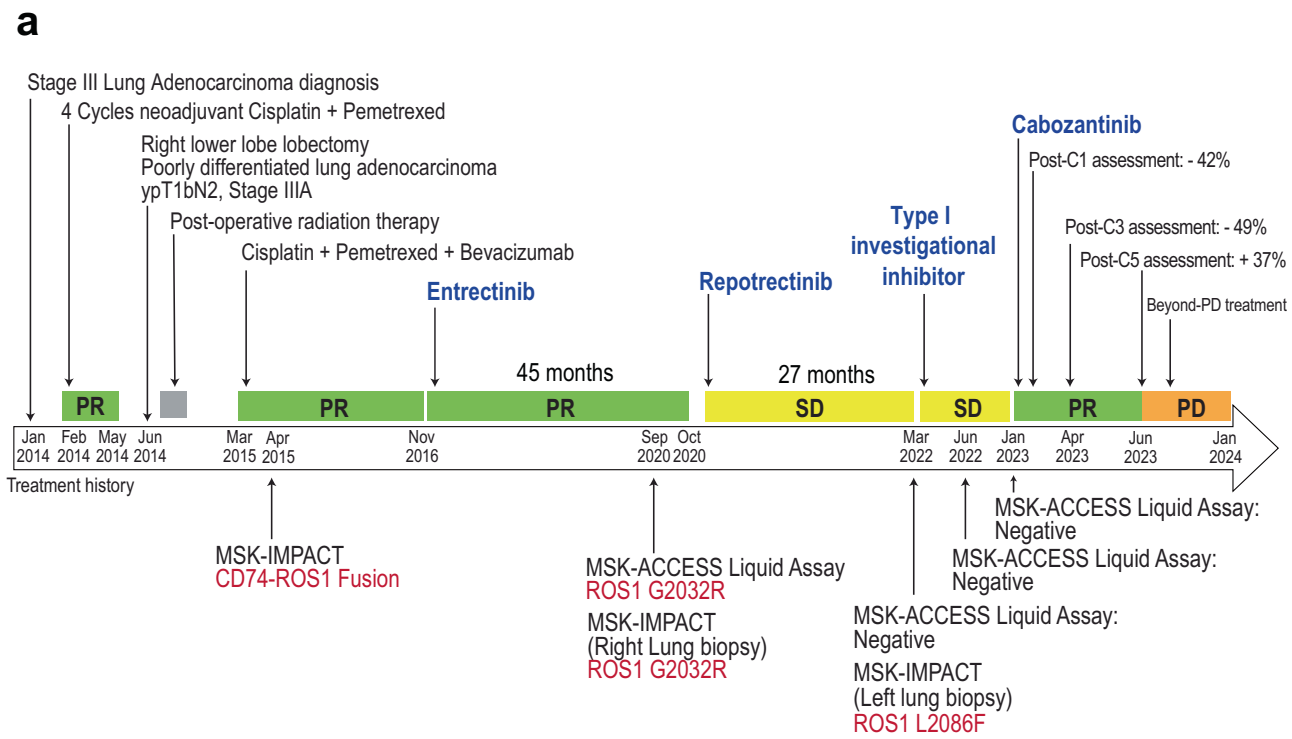

Fig. 4 | Clinical course of a patient with ROS1 fusion-positive non-small cell lung carcinoma. a Timeline of the diagnostic and treatment history of the patient which exhibits initial response to cabozantinib. Periods of partial response (PR) are shown in light green, metabolic complete response (CR) is shown in green, and stable disease is shown in yellow. **b** Images of chest CT showing partial response to treatment with cabozantinib.

range to form π–π stacking interaction similarly to observations with gilteritinib (Supplementary Fig. 7).

Clinical activity of non-type I TKIs in ROS1 L2086F positive NSCLCs

To further investigate the role of drug repurposing to address ROS1 L2086F resistance mutations in the clinical setting, we queried institutional electronic medical records at Memorial Sloan Kettering Cancer Center (MSKCC) to identify patients with acquired ROS1 L2086F mutation following treatment with ROS1 macrocyclic inhibitors. This retrospective query identified four patients, with two of them subsequently enrolled in the prospective phase 2 clinical trial (NCT01639508; IRB 12-097) evaluating cabozantinib efficacy in individuals with advanced NSCLC at MSKCC. This basket trial aims to investigate the role of the type II inhibitor cabozantinib in targeting various acquired resistance mutations based on compelling clinical or preclinical evidence of actionability.

Case #1. A 49-year-old otherwise healthy never-smoker patient was diagnosed with stage IIIA (ypT1bN2) poorly differentiated lung adenocarcinoma in 2014. The patient received neoadjuvant cisplatin and pemetrexed, followed by right lower lobe lobectomy, and post-operative radiation therapy. In 2015, due to disease recurrence, the patient received first-line cisplatin, pemetrexed, and bevacizumab with a PR, followed by pemetrexed and bevacizumab maintenance treatment. During chemotherapy, MSK-IMPACT was performed on the surgical specimen, and CD74–ROS1 fusion was identified (Fig. 4a).

The patient then received entrectinib (a type-I inhibitor) from November 2016 to October 2020 with a PR and subsequent PD. Upon PD, both tissue and plasma samples were acquired and analyzed with MSK-IMPACT and MSK-ACCESS (FDA-approved plasma ctDNA NGS). Both assays identified an acquired solvent-front ROS1 G2032R mutation. Based on this finding, the patient was subsequently treated with repotrectinib (a type-I macrocyclic inhibitor) for 1 year and 5 months. Upon disease progression on repotrectinib, both tumor and plasma samples were acquired. While circulating tumor (ct)DNA sequencing was negative, tumor sequencing identified loss of the solvent-front ROS1 G2032R mutation and emergence of the CS6 ROS1 L2086F mutation.

The patient was subsequently enrolled in a clinical trial assessing a new type-I ROS1 selective inhibitor for 10 months. MSK-ACCESS at disease progression in early 2023 was, unfortunately, negative for detectable somatic alterations. Based on the prior identification of the ROS1 L2086F mutation, the patient was enrolled in a prospective, phase 2 trial of cabozantinib. A RECIST 1.1 partial response (−42% target lesions shrinkage and a dramatic improvement in lymphangitic disease) was achieved after just 4 weeks of therapy, along with a clinical response marked by an improvement in pre-cabozantinib dyspnea. A confirmed partial response was observed on subsequent imaging after 2 months (49% tumor shrinkage, nadir, Fig. 4b).

Treatment with cabozantinib required a dose reduction from 60 mg daily to 40 mg daily for asthenia, and no major tolerability issues were identified thereafter. After 4 months of therapy, asymptomatic radiological evidence of disease progression was observed with slowly growing pulmonary disease. Due to the overall modest increase in tumor burden, and the enduring clinical benefit reported by the patient, the patient was kept on cabozantinib therapy and remains on the clinical trial more than 12 months into treatment.

Case #2. A 70-year-old patient without a smoking history was diagnosed with stage IV NSCLC in 2016 and received first-line carboplatin and pemetrexed treatment from September 2016 to April 2017. Following the identification of CD74–ROS1 fusion, the patient was switched to crizotinib (type I inhibitor) and had a partial response (PR) for almost 3 years with subsequent progressive disease (PD). Following progression, the patient was treated with repotrectinib (type I macrocyclic inhibitor) and responded for 1 year and 2 months, however, PD was later observed.

A right lower lobe biopsy of a progressing lesion was collected and analyzed with MSK-IMPACT, an FDA-approved next-generation sequencing assay designed for fixed paraffin-embedded samples. This resulted in the identification of an acquired ROS1 L2086F resistance mutation. The patient then received cabozantinib (a type II inhibitor) in the same phase 2 trial. The patient's previously progressive disease stabilized with cabozantinib [best response of stable disease (SD) per RECIST1.1], with a total time on therapy of almost 5 months. The treatment was moderately well tolerated but was complicated by renal infarction, which required investigational treatment interruption and subsequent dose reduction. Cabozantinib was ultimately discontinued due to RECIST1.1 PD; the patient did not receive additional treatments.

Discussion

The study of kinase-intrinsic resistance has been crucial to improving outcomes in patients with advanced, fusion-driven cancers. Joining *BCR-ABL*-positive chronic myelogenous leukemia and *ALK* fusion-positive NSCLCs, *ROS1* fusion-positive NSCLCs are a recent example of how sequential TKI therapy (i.e., using repotrectinib in TKI pre-treated patients) can extend the total duration of disease control for an individual. Notably, the patterns of on-target or kinase intrinsic resistance tend to reflect the TKI-binding mode-driven selection pressure, wherein cases treated with type I inhibitors showed the prevalence of the solvent front, ROS1 G2032R mutation to date. On target resistance is driven by the expansion of tumor cells harboring TKI type-specific resistant mutations. While repotrectinib, with activity on ROS1 G2032R resistance, is the only approved second-line TKI option, other inhibitors such as taletrectinib and NVL-520 are also highly active and may be approved in the future. The increasing use of next-generation TKI therapy is likely to shift emergent resistance patterns.

In this study, we present preclinical and clinical data supporting the hypothesis that ROS1 L2086F acts as a convergent liability for type I ROS1 TKIs, including those that are approved (crizotinib, entrectinib, repotrectinib), listed in guidelines (lorlatinib), and investigational agents such as taletrectinib. The ROS1 L2086F mutation also confers resistance to the novel ROS1-selective, TRK-sparing inhibitor, NVL-520[11]. Here, we compared the activity of the type II inhibitor cabozantinib with gilteritinib, which is best known as a type I FLT3 inhibitor approved by the FDA for treating adults with FLT3-mutant acute myeloid leukemia.

As a prototypic type II inhibitor, cabozantinib binding is unaffected by solvent front mutations such as ROS1 G2032R and the recalcitrant catalytic-spine 6 mutation, ROS1 L2086F. Gilteritinib exhibits resistance to ROS1 G2032R. However, due to its specific binding pocket occupancy within the ROS1 kinase domain, it remains unaffected by ROS1 L2086F. The ROS1 compound mutation studies underscore gilteritinib's potential as a salvage therapy in scenarios involving acquisition of F2004C + L2086F compound mutation after sequential treatments. Despite its lower overall potency for ROS1, in the context of F2004C + L2086F, it stands as the sole viable option in the current pharmacology landscape. One limitation of our study is the absence of in vivo investigation into gilteritinib activity in ROS1 L2086F mutant patient-derived xenografts. Considering the unique pharmacokinetic profiles of these agents, our future experiments will specifically address these questions.

Okada et al.[17] discovered that ALK L1256F, a paralog of ROS1 L2086F, introduces an aromatic ring at the CS6 residue. This aromatic ring can engage in π–π interactions with inhibitor molecules. Mutation of the leucine residue to phenylalanine in the resistant mutant protein is permissive to gain of these new π–π stacking interactions, which is predicted to enhance the F2086 mutant sensitivity to alectinib, as compared to wildtype L2086. As seen in the case of cabozantinib and gilteritinib interaction with ROS1, alectinib does not encircle the ALK CS6 residue at a downward fixed angle akin to crizotinib and lorlatinib. Instead, it positions an aromatic ring system over the CS6 mutation. Based our modeling results, in vitro and patient results, we hypothesize that an additional mediator of the enhanced sensitivity of the ROS1 L2086F mutation to cabozantinib and gilteritinib might lie in the introduction of π–π interaction with these inhibitors.

To assess the utility of these agents in mitigating ROS1 L2086F resistance, it is imperative to consider toxicity and pharmacokinetic (PK) parameters in relation to effective inhibitory concentrations for both cabozantinib and gilteritinib. While cabozantinib primarily targets KDR, and gilteritinib targets FLT3, neither inhibitor is selective, exhibiting nanomolar potency for multiple kinases (Supplementary Fig. 8). Adverse events reported in the CELESTIAL (cabozantinib[28]) and ADMIRAL (gilteritinib[29]) clinical trials (Supplementary Table S1) underscore the largely non-overlapping toxicities of these inhibitors, likely due to their distinct spectrum of kinase inhibitory profiles. The most frequent grade 3 or higher events uniquely observed in cabozantinib-treated patients were palmar-plantar erythrodysesthesia and hypertension, whereas gilteritinib-treated patients experienced a high incidence of hematological events, including febrile neutropenia, anemia, and thrombocytopenia. The higher incidence of hematologic cell dysfunctions in patients treated with gilteritinib may be partly due to the fact that these patients have acute myeloid leukemia, which predisposes them to cytopenias. Additionally, the critical role of FLT3, expressed by immature hematopoietic cells, in the normal development of stem cells and the immune system may contribute to this profile.

Based on the pharmacokinetic (PK) data from the FDA prescribing information and the CHRYSALIS study, gilteritinib may be a less effective clinical option for the mitigation of $ROS1^{L2086F}$-driven resistance[30]. At the recommended daily oral dosage of 120 mg, the steady-state maximum concentration (Cmax) of total (bound and unbound) gilteritinib in plasma is 306 nM. On-target inhibition of $ROS1^{L2086F}$ in CUTO-28 cells necessitated ~250 nM inhibitor (Supplementary Fig. 9). However, the steady-state area under the curve (AUC) of gilteritinib offers exposure that is 50 times higher

than the cell-based IC_{50}, which may provide a viable option when cabozantinib toxicity is intolerable.

Cabozantinib is inherently more potent than gilteritinib, achieving over 90% inhibition of $ROS1^{L2086F}$ at a 25 nM dose in CUTO-28 cells. According to PK data reported by Nguyen et al., the steady-state plasma Cmax of total drug levels at the recommended dose of 60 mg daily is 2200 nM[31], which is 80–90 times higher than the concentration needed to inhibit CUTO-28 $ROS1^{L2086F}$.

Cerbone et al.[32] described the therapeutic window for cabozantinib using real-world clinical data, identifying a minimum effective concentration of 536.8 ng/ml and a toxicity threshold at 617.2 ng/ml, presenting a narrow therapeutic range of approximately 80 ng/ml. These findings reflect clinical observations regarding cabozantinib's adverse events and suggest that it can be a highly effective inhibitor but with a significant risk of adverse effects. Consequently, dose de-escalation of cabozantinib is often employed. Utilizing data from Nguyen et al., we determined that even with dose reductions to 20 or 40 mg, cabozantinib pharmacokinetics still show potentially effective steady-state Cmax concentrations of 376 and 184 nM, respectively, which are 5–10 times the concentration needed to achieve near-complete ROS1 L2086F inhibition (Supplementary Fig. 9).

The overarching observation is that TKI type switching is a legitimate method of abrogating select pan type I TKI kinase-intrinsic resistance in ROS1 fusion-driven NSCLC. In contrast to type I TKIs, type II TKIs bind a hydrophobic pocket adjacent to the ATP-binding region when the kinase activation loop (A-loop) adopts the "DFG-out" conformation, thus bypassing the solvent front mutations that pose challenges for type I inhibitors. We and others previously demonstrated the benefits of type II TKI use with ROS1 D2033N resistance, and in *NTRK* fusion-positive cancers that acquire xDFG (TRKA G667, TRKC G696) resistance substitutions that stabilize the DFG-out conformation. Gilteritinib was active against the ALK L1256F resistance mutation in *ALK* fusion-positive NSCLCs, and against select D1228 resistance substitutions in MET-driven cancers that progressed on prior type I TKI therapy[18]. Hence, sequencing-informed TKI-type switching has the potential to improve outcomes and provide effective therapeutic interventions in many resistance-driven cancer settings[33].

Unfortunately, in fusion-positive cancers, few rationally designed next-generation type II inhibitors have been developed. All approved agents for any fusion-positive cancer (e.g., involving *ALK, RET, ROS1, NTRK1/2/3, FGFR1/2/3*) are type I drugs. The successful development of novel type II inhibitors may thus provide a transformative opportunity for targeting kinase-intrinsic resistance.

Methods

Cell culture

Ba/F3 cells were purchased from DSMZ German Collection of Microorganisms and Cell Cultures, GmBH (Catalog # ACC 300). NIH3T3 cells were purchased from the American Type Culture Collection (Catalog # CRL-1658). CUTO-28 cells were obtained as part of a research agreement from the University of Colorado, following Institutional Review Board approved informed consent of the patient, and has been described by McCoach et al. [34]. CUTO-28 cells were cultured in RPMI medium 1640 with 10% (vol/vol) FBS, 2 mmol/L L-glutamine, penicillin, streptomycin, and amphotericin B. Parental Ba/F3 cells were cultured in RPMI medium 1640 with 10% (vol/vol) FBS, 2 mmol/L L-glutamine, penicillin, streptomycin, amphotericin B and 2 ng/mL recombinant murine IL-3. NIH3T3 cells were cultured in DMEM medium with 10% (vol/vol) CS, 2 mmol/L L-glutamine, penicillin, streptomycin, and amphotericin B. All cells were tested for mycoplasma at least every three months by using the Lonza MycoAlert™ PLUS Kit.

Ba/F3 and NIH3T3 cell lines

Generation of Ba/F3 stable cell lines has been described[2]. Cell lines were maintained at densities of 0.5×10^6 to 1.5×10^6 /mL and infected with retrovirus-encoding human *CD74-ROS1* and *EZR-ROS1* fusion genes. *CD74-ROS1* and *EZR-ROS1* fusions with F2004C, L2026M, G2032R, and L2086F mutations were made using site-directed mutagenesis following the manufacturer's protocol (Agilent) using primers listed in Supplementary Table S2. Platinum-E cells (Cell Biolabs, Inc.) were transfected with pBABE *CD74-ROS1* or pCX4 *EZR-ROS1* wild-type or mutant constructs using Biotool DNA transfection reagent to generate replication incompetent, ecotropic retrovirus. Parental NIH3T3 cells were seeded at 50% confluence and infected with retrovirus. Cells were selected with puromycin treatment (2 μg/mL) for 72–96 h prior to being used for experimental work. Transformed Ba/F3 cell lines: For IL-3 withdrawal, the cells were washed three times with complete medium without IL-3, and seeded at 0.5×10^6 cells per mL in RPMI medium 1640 with 10% (vol/vol) FBS, 2 mmol/L L-glutamine, penicillin, streptomycin, amphotericin B without supplemented IL-3. Cells were counted every 2 days until the population had at least tripled, indicating that the proliferating population was IL-3 independent. Sanger sequencing of integrated cDNA in the transformed cell lines was done to verify the presence of the desired mutation. For this, DNA was harvested from cell pellets using QuickExtract DNA Extraction Solution (Lucigen). The ROS1 kinase and C-terminal domains were PCR amplified using the primers ROS1 5707F (5′-GACAAAGAGTTGGCTGAGCTG-3′) and ROS1 REV_14 (5′-TCAGACCCATCTCCATATCCA-3′) and bidirectionally sequenced using the primers ROS1 6198F (5′-CTGTGTCT ACTTGGAACGGATG-3′) and ROS1 6304R (5′-TCTCTGGCGAGTC CAAAGTC-3′). Chromatographs were aligned using Benchling software to verify that the correct mutation was present and that no other mutations were introduced during viral transduction.

Generation of mutated patient-derived cell line

The CUTO-28 cell line is a patient-derived cell line harboring a *TPM3–ROS1* fusion, authenticated by short tandem repeat (STR) analysis by the Barbara Davis Center Molecular Biology Service Center at the University of Colorado[23] and was a gift from the laboratory of Dr. Robert Doebele. A CRISPR-Cas9 genome-engineered CUTO28 cell line with an endogenous L2086F mutation was engineered. A pX330 vector was made to express a guide directed to the L2086 region of ROS1. A homology-directed repair (HDR) oligo template was designed to have 80 base pairs of homology on each side of the Cas9 cut site with a single base pair substitution allowing for the desired mutation and alteration of the PAM site. CUTO28 cells were plated at a density of 500,000 cells per well in a 6-well plate, 24 h prior to transfection, then transfected with either GFP alone or 1 μg pX330(I) L2086F guide and 10 μg HDR Oligo. Forty-eight hours later, the media was removed and replaced with RPMI1640 10% Fetal Bovine Serum 1% penstrep 1% L glutamine (R10) containing 500 nM lorlatinib and 500 nM crizotinib and allowed to grow out. Media with these inhibitors was changed every 72–96 h. On day 16, cells were placed in inhibitor-free media and allowed to grow in R10. Lucigen QuickExtract reagent was used to generate genomic DNA, and RNA was generated using the Qiagen RNeasy kit, followed by cDNA synthesis using Applied Biological Materials (ABM) All in one 5× Master Mix. Genomic DNA and cDNA were used in polymerase chain reaction to amplify a region of interest containing the L2086 codon. Sanger sequencing of the PCR amplicons was used to confirm the genomic edit, leading to achieving the desired codon change. Guide DNA, HDR, and PCR primer sequences are reported in Supplementary Table S2.

Cell viability assays

All inhibitors were prepared as 1 mM stocks in dimethyl sulfoxide (DMSO). Inhibitors were distributed at 2× indicated final concentrations into 384-well plates pre-seeded with 25 μL per well of complete medium using a D300 Digital Dispenser (Hewlett-Packard). Ba/F3 cells expressing wild-type or mutant *CD74-ROS1* constructs were seeded at 1000 cells per well in a volume of 25 μL using a Multidrop Combi Reagent Dispenser (Thermo Fisher Scientific). Plates were incubated for 72 h at 37 °C, 5% CO_2. Viability was measured using the cell counting kit-8 (CCK-8, Bimake) and read on a Biotek Synergy 2 plate reader. Each condition was assayed in triplicate. Data were normalized using Microsoft Excel, and IC_{50} values were calculated using a nonlinear regression analysis in GraphPad Prism.

Colony formation assays

Plates were pre-seeded with 0.4% agarose in the complete medium [DMEM with 10% (vol/vol) calf serum, 2 mM L-glutamine, penicillin, streptomycin, and amphotericin B] with indicated concentrations of each inhibitor. Each inhibitor had its own paired DMSO (vehicle) control condition. NIH3T3 cells expressing *CD74-ROS1* or *EZR-ROS1* wild-type or L2086F were plated in 0.2% agarose in complete medium with indicated concentrations of each inhibitor at a density of 8000 cells per 0.5 mLs of agarose; 24 h after plating 1 mL of complete medium with indicated concentrations of each inhibitor was added to each well to prevent dehydration of the agarose. Plates were read 4 weeks after seeding using a GelCount (Oxford Optronix). Colony counts were determined for each well using the GelCount software and normalized to the average colony count from the paired DMSO condition for each inhibitor. Data analysis and visualization were performed using Microsoft Excel and GraphPad Prism.

Immunoblot analysis

Ba/F3 and CUTO-28 cells were treated with the indicated concentrations of inhibitors for indicated duration, prior to harvest. Ba/F3 cell lines and CUTO28 cells were pelleted, washed with ice-cold phosphate-buffered saline (PBS), and lysed in cell lysis buffer supplemented with 0.25% deoxycholate, 0.05% SDS, and protease and phosphatase inhibitors. Protein concentration was determined using the Pierce BCA Protein Assay Kit (Thermo Fisher Scientific). After protein quantification, lysates were extracted with Laemmli sample buffer for 10 min at 75 °C and lysates were run on 4% to 12% Bis–Tris gels (Invitrogen; Thermo Fisher Scientific). Proteins were transferred to nitrocellulose membranes (Prometheus) and probed with phospho-ROS1 Y2274 (cat. # 3078; 1:1000; Cell Signaling Technology), ROS1 (cat. # 3287; 1:1000; Cell Signaling Technology), phospho-p44/42 MAPK (cat. #9101 or #4370; 1:1000, Cell Signaling Technology), ERK2 (cat. # sc-1647; 1:1000; Santa Cruz Biotechnology), GAPDH (cat. # TA802519; 1:5000; Origene), phospho-STAT3 (cat. #9145; 1:1000, Cell Signaling Technology), STAT3 (cat. #9139; 1:1000, Cell Signaling Technology), phospho-SHP2 (cat. # A5278; 1:1000, SelleckChem), SHP2 (cat. #3397; 1:1000, Cell Signaling Technology), phospho-S6 (cat. #4858 1:1000, Cell Signaling Technology), S6 (cat. #2317; 1:1000, Cell Signaling Technology), and Actin (cat. # JLA20; 1:5000; Developmental Studies Hybridoma Bank). The signal was detected using a BioRad ChemiDoc imaging station or an LI-COR Odyssey imaging system with the use of HRP-conjugated or IR dye secondary antibodies, respectively. Blots were derived from the same experimental lysates, and the majority were processed in parallel. In rare cases where technical failure resulted in poor blot quality, we re-ran the same lysates on new gels, thus the data represent the same experiment. All raw data from western blot exhibits in the Figures are shown in Supplementary Fig. 10.

Structural modeling

The chemical structures of gilteritinib and cabozantinib were downloaded from PubChem to be employed in docking simulations. Protein complexes 6JQR and 7AB1, which feature Gilteritinib in complex with FLT3 and MerTK kinases, respectively, were retrieved from the Protein Data Bank (PDB) to serve as structural references during the docking result analysis phase. Due to the absence of cabozantinib complexes in PDB, the 6SD9 complex of the closely related quinoline-based type II inhibitor foretinib with MET was obtained from PDB to be used as the closest available reference.

For the target ROS1 kinase, the active conformation (DFG-in) was obtained from PDB (3ZBF), while its inactive state was acquired from previous structural modeling experiments where it was built using ALK (PDB entry 4FNY) DFG-out as a structural template[35]. The ROS1 L2086F and G2032R mutations were introduced both on the active DFG-in and on the inactive DFG-out ROS1 structures through single amino-acid substitution using PyMOL version 2.5.3. Subsequently, target protein structures were prepared using the Schrödinger Suite, and any missing loops or hydrogen atoms were added.

Docking was performed with Glide in Schrödinger Maestro Version 12.7.161. A 30-angstrom grid box was centered around both the WT L2086 and the mutant L2086F CS6 residue. Based on the analysis of gilteritinib and foretinib reference binding poses, hydrogen bonding constraints were placed. For gilteritinib, the generation of at least 1 hydrogen bond with either hinge 1 (H1) E2027 or hinge 3 (H3) M2029 peptide backbone was placed, while for cabozantinib generation of a hydrogen bond with H1 residue was required.

Ligands were prepared using the Ligprep and docking simulations were performed using the Glide module in standard precision mode, with the pre-specified hydrogen bonding constraints. Successful binding poses were analyzed and the best scoring ones were selected[36].

Murine model studies

All animal model studies were conducted in accordance with the Animal Welfare Act (AWA), Public Health Service (PHS), the United States Department of Agriculture (USDA), and under the auspices of an approved protocol from the OHSU Institutional Animal Care and Use Committee (IACUC). Four- to six-week-old female athymic nude mice (Nu/J, Strain # 002019, RRID:IMSR_JAX:002019) were purchased from The Jackson Laboratory (Bar Harbor, ME) and housed and handled under specific pathogen-free conditions in the Oregon Health & Science University's animal care facilities. After an initial 2-week environmental adjustment period, mice were placed under anesthesia using 2% isoflurane/oxygen, weighed, and ear punched for identification purposes. Tumor cells (1×10^6 were mixed with 50 µl of matrigel and injected subcutaneously into the left or right flank. Animals were allowed to recover under supervision before being returned to animal facilities. Injected animals were checked daily until tumors were palpable nodules, at which time both animal weight and tumor size were measured thrice weekly using balance and a digital caliper (cat 14-648-17, Fisher Scientific, Federal Way, WA). Tumor volume was estimated using caliper measurements, based on the ellipsoid volume formula ($\pi/6 \times D3$). TKI treatment began ~12–14 days after initial injection when animals were randomized to TKI treatment groups. The study was not blinded. Both gilteritinib and cabozantinib treatment groups were administered indicated TKI at 30 mg/kg formulated in 0.5% methylcellulose, once daily via oral gavage for ten days. Vehicle (0.5% methylcellulose) treated tumors were allowed to grow until they reached the humane limit of 1500–2000 mm^3, at which time animals were sacrificed in accordance with IACUC protocol. Specifically, animals were deeply anesthetized using isoflurane prior to euthanasia. The method of euthanasia involved cervical decapitation, performed only when the animals were confirmed to be fully anesthetized and unconscious, in accordance with AVMA Guidelines for the Euthanasia of Animals. Experimental endpoints were carefully defined and included criteria such as significant weight loss (greater than 20% of body weight), signs of severe distress or pain unrelievable by analgesics, tumor size exceeding ethical limits (typically greater than 10% of the body weight or causing functional impairment), and any signs of systemic illness or failure to thrive. Monitoring was conducted daily to ensure early detection of these endpoints, and animals meeting any of these criteria were promptly euthanized to prevent unnecessary suffering.

Patient clinical cases

The patients described in this analysis were treated in the prospective phase 2 clinical trial NCT01639508 (IRB 12-097) and provided written informed consent for all procedures described and publication of genomic findings and outcomes. All sample acquisition and sequencing were performed within the scope of the prospective Institutional clinical sequencing trial NCT01775072 (IRB 12-245). Both trials are approved by the institutional review board of Memorial Sloan Kettering Cancer Center and conducted according to the ethical guidelines of the Declaration of Helsinki.

Statistical analyses

In all graphs, mean ± standard error of means is shown unless otherwise stated with a minimum of three technical replicates. A two-way ANOVA with multiple comparison tests was used to assess significant differences in tumor volumes in the vivo study. P values < 0.05 were deemed statistically significant. In vivo studies employed one-way ANOVA with Dunnett's multiple comparison test. All data were initially analyzed using Microsoft Excel. GraphPad Prism v9.3 software was used for statistical analysis and plotting graphs.

Data availability

Raw data associated with functional assays reported herein is available here: https://doi.org/10.6084/m9.figshare.26166898. Engineered Ba/F3 or NIH3T3 cell lines will be shared through MTA agreements in compliance with our institutions.

Received: 12 January 2024; Accepted: 22 July 2024;
Published online: 08 August 2024

References

1. Yu, Z.-Q. et al. ROS1-positive non-small cell lung cancer (NSCLC): biology, diagnostics, therapeutics and resistance. *J. Drug Target.* **30**, 845–857 (2022).
2. Keddy, C. et al. Resistance profile and structural modeling of next-generation ROS1 tyrosine kinase inhibitors. *Mol. Cancer Ther.* **21**, 336–346 (2022).
3. Davare, M. A. et al. Structural insight into selectivity and resistance profiles of ROS1 tyrosine kinase inhibitors. *Proc. Natl Acad. Sci. USA* **112**, E5381–E5390 (2015).
4. Mazieres, J. et al. Immune checkpoint inhibitors for patients with advanced lung cancer and oncogenic driver alterations: results from the IMMUNOTARGET registry. *Ann. Oncol.* **30**, 1321–1328 (2019).
5. Shaw, A. T. et al. Crizotinib in ROS1-rearranged advanced non-small-cell lung cancer (NSCLC): updated results, including overall survival, from PROFILE 1001. *Ann. Oncol.* **30**, 1121–1126 (2019).
6. Drilon, A. et al. Entrectinib in ROS1 fusion-positive non-small-cell lung cancer: integrated analysis of three phase 1–2 trials. *Lancet Oncol.* **21**, 261–270 (2020).
7. Drilon, A. et al. Repotrectinib (TPX-0005) is a next-generation ROS1/TRK/ALK inhibitor that potently inhibits ROS1/TRK/ALK solvent- front mutations. *Cancer Discov.* **8**, 1227–1236 (2018).
8. Nagasaka, M. et al. TRUST-II: a global phase II study of taletrectinib in ROS1-positive non-small-cell lung cancer and other solid tumors. *Fut. Oncol.* **19**, 123–135 (2023).
9. Katayama, R. et al. The new-generation selective ROS1/NTRK inhibitor DS-6051b overcomes crizotinib resistant ROS1-G2032R mutation in preclinical models. *Nat. Commun.* **10**, 3604 (2019).
10. Papadopoulos, K. P. et al. U.S. phase I first-in-human study of taletrectinib (DS-6051b/AB-106), a ROS1/TRK inhibitor, in patients with advanced solid tumors. *Clin. Cancer Res.* **26**, 4785–4794 (2020).
11. Drilon, A. et al. NVL-520 is a selective, TRK-sparing, and brain-penetrant inhibitor of ROS1 fusions and secondary resistance mutations. *Cancer Discov.* **13**, 598–615 (2023).
12. Lin, J. J. et al. Spectrum of mechanisms of resistance to crizotinib and lorlatinib in ROS1 fusion–positive lung cancer. *Clin. Cancer Res.* **27**, 2899–2909 (2021).
13. Drilon, A. et al. ROS1-dependent cancers—biology, diagnostics and therapeutics. *Nat. Rev. Clin. Oncol.* **18**, 35–55 (2021).
14. Weber, U., Davies, K. D. & Camidge, D. R. L2086F mutant ROS1 rearranged NSCLC resistant to repotrectinib responds to cabozantinib: a case report. *JTO Clin. Res. Rep*. **5**, 100673 (2024).
15. Sakamoto, M. & Patil, T. Exceptional response to lorlatinib and cabozantinib in ROS1-rearranged NSCLC with acquired F2004V and L2086F resistance. *NPJ Precis. Oncol.* **7**, 56 (2023).
16. Roskoski, R. Classification of small molecule protein kinase inhibitors based upon the structures of their drug-enzyme complexes. *Pharmacol. Res.* **103**, 26–48 (2016).
17. Okada, K. et al. Prediction of ALK mutations mediating ALK-TKIs resistance and drug re-purposing to overcome the resistance. *eBioMedicine* **41**, 105–119 (2019).
18. Mizuta, H. et al. Gilteritinib overcomes lorlatinib resistance in ALK-rearranged cancer. *Nat. Commun.* **12**, 1261 (2021).
19. Cohen, P., Cross, D. & Jänne, P. A. Kinase drug discovery 20 years after imatinib: progress and future directions. *Nat. Rev. Drug Discov.* **20**, 551–569 (2021).
20. Hata, A. et al. Complex mutations in the epidermal growth factor receptor gene in non-small cell lung cancer. *J. Thorac. Oncol.* **5**, 1524–1528 (2010).
21. Recondo, G. et al. Diverse resistance mechanisms to the third-generation ALK inhibitor lorlatinib in ALK-rearranged lung cancer. *Clin. Cancer Res.* **26**, 242–255 (2020).
22. Yakes, F. M. et al. Cabozantinib (XL184), a novel MET and VEGFR2 inhibitor, simultaneously suppresses metastasis, angiogenesis, and tumor growth. *Mol. Cancer Ther.* **10**, 2298–2308 (2011).
23. Tyler, L. C. et al. MET gene amplification is a mechanism of resistance to entrectinib in ROS1+ NSCLC. *Thorac. Cancer* **13**, 3032–3041 (2022).
24. Pflug, A. et al. A-loop interactions in Mer tyrosine kinase give rise to inhibitors with two-step mechanism and long residence time of binding. *Biochem. J.* **477**, 4443–4452 (2020).
25. Kawase, T. et al. Effect of Fms-like tyrosine kinase 3 (FLT3) ligand (FL) on antitumor activity of gilteritinib, a FLT3 inhibitor, in mice xenografted with FL-overexpressing cells. *Oncotarget* **10**, 6111–6123 (2019).
26. Jin, M. Y. et al. Engineered non-covalent π interactions as key elements for chiral recognition. *Nat. Commun.* **13**, 3276 (2022).
27. Zhao, Y. et al. Conformational preferences of π–π stacking between ligand and protein, analysis derived from crystal structure data geometric preference of π–π interaction. *Interdiscip. Sci. Comput. Life Sci.* **7**, 211–220 (2015).
28. Abou-Alfa, G. K. et al. Cabozantinib in patients with advanced and progressing hepatocellular carcinoma. *N. Engl. J. Med.* **379**, 54–63 (2018).
29. Perl, A. E. et al. Gilteritinib or chemotherapy for relapsed or refractory FLT3-mutated AML. *N. Engl. J. Med.* **381**, 1728–1740 (2019).
30. James, A. J. et al. Pharmacokinetic profile of gilteritinib: a novel FLT-3 tyrosine kinase inhibitor. *Clin. Pharmacokinet.* **59**, 1273–1290 (2020).
31. Nguyen, L., Benrimoh, N., Xie, Y., Offman, E. & Lacy, S. Pharmacokinetics of cabozantinib tablet and capsule formulations in healthy adults. *Anticancer. Drugs* **27**, 669 (2016).
32. Cerbone, L. Association of cabozantinib pharmacokinetics, progression and toxicity in metastatic renal cell carcinoma patients: results from a pharmacokinetics/pharmacodynamics study. *ESMO Open*. **6**, 100312 (2021).
33. Fujino, T. et al. Foretinib can overcome common on-target resistance mutations after capmatinib/tepotinib treatment in NSCLCs with MET exon 14 skipping mutation. *J. Hematol. Oncol.* **15**, 79 (2022).
34. McCoach, C. E. et al. Resistance mechanisms to targeted therapies in ROS1+ and ALK+ non–small cell lung cancer. *Clin. Cancer Res.* **24**, 3334–3347 (2018).
35. Drilon, A. et al. A novel crizotinib-resistant solvent-front mutation responsive to cabozantinib therapy in a patient with ROS1-rearranged lung cancer. *Clin. Cancer Res.* **22**, 2351–2358 (2016).
36. Repasky, M. P., Shelley, M. & Friesner, R. A. Flexible ligand docking with Glide. *Curr. Protoc. Bioinforma*. **Chapter 8**, Unit 8.12 (2007).

Acknowledgements

We extend our gratitude to Dr. Clare Wilhelm for his invaluable assistance with paper editing and management. The study was funded by the Medical

Research Foundation of Oregon Early Career Investigator Award (RT), NIH/NCI R01CA233495 (Davare), NIH/NCI P30CA008748 (Repetto, Harada, Drilon), NIH/NCI R01CA273224 (Drilon).

Author contributions

R.T. and M.R. contributed equally. Conceptualization: M.A.D. and A.D.; Methodology and experimentation: R.T., M.R., C.K., K.N., K.J., C.Z.B., G.H., A.D. and M.A.D.; Data analysis: R.T., M.R., C.K., K.N., A.D. and M.A.D.; Writing (Original, Review, Editing): R.T., M.R., A.D., and M.A.D.; Project Administration: A.D. and M.A.D.; Funding Acquisition: R.T., G.H., A.D., and M.A.D.

Competing interests

Dr. Drilon reports Honoraria/Advisory Boards: 14ner/Elevation Oncology, Amgen, Abbvie, ArcherDX, AstraZeneca, Beigene, BergenBio, Blueprint Medicines, Chugai Pharmaceutical, EcoR1, EMD Serono, Entos, Exelixis, Helsinn, Hengrui Therapeutics, Ignyta/Genentech/Roche, Janssen, Loxo/Bayer/Lilly, Merus, Monopteros, MonteRosa, Novartis, Nuvalent, Pfizer, Prelude, Repare RX, Takeda/Ariad/Millenium, Treeline Bio, TP Therapeutics, Tyra Biosciences, Verastem; Associated Research to Institution: Foundation Medicine, Teva, Taiho, GlaxSmithKlein; Equity: mBrace, Treeline; Copyright: Selpercatinib-Osimertinib (pending); Royalties: Wolters Kluwer, UpToDate, Food/Beverage: Boehringer Ingelheim, Merck, Puma: CME Honoraria: Answers in CME, Applied Pharmaceutical Science, Inc., AXIS, Clinical Care Options, EPG Health, Harborside Nexus, I3 Health, Imedex, Liberum, Medendi, Medscape, Med Learning, MJH Life Sciences, MORE Health, Ology, OncLive, Paradigm, Peerview Institute, PeerVoice, Physicians Education Resources, Remedica Ltd., Research to Practice, RV More, Targeted Oncology, TouchIME, WebMD. Dr. Davare reports consulting for Nuvalent. The remaining authors declare no competing interests.

Additional information

Supplementary information The online version contains supplementary material available at https://doi.org/10.1038/s41698-024-00663-1.

Correspondence and requests for materials should be addressed to Alexander Drilon or Monika A. Davare.